ELSEVIER

Materials Science and Engineering C 11 (2000) 145–153

MATERIALS SCIENCE & ENGINEERING C

www.elsevier.com/locate/msec

Growth dynamics of red abalone shell: a biomimetic model

Thomas Graham, Mehmet Sarikaya *

Materials Science and Engineering, University of Washington, Seattle, WA 98195, USA

Received 24 September 1998; received in revised form 14 August 2000; accepted 14 August 2000

Abstract

A model of shell formulation was developed in red abalone in which the nacre forms over the prismatic section. The model was based on roughness variations of the growing edge of the mollusc determined by atomic force microscopy. These variations were spatially distinguished and related to various sections of the shell, i.e., nacreous, prismatic, and the interface in between. With a diffusional growth model, it was estimated that for a relatively rough, $z_{rms} = (1.34 \pm 0.23)$ μm, surface, it will take (16.5 ± 2.5) days for this surface to become flat, $z_{rms} = 1$ nm. This is the time it takes what was once a rough prismatic surface eventually smoothening to become a nacreous layer. For this time interval, the shell will have grown radially by approximately 1.2 mm. The smoothening coefficient, which measures the rate at which the nacre forms over the prismatic surface, was found to be $\varepsilon_s = (0.042 \pm 0.005)$ μm^2/day. The model may have implications both for better understanding of biological hard tissue formation and their biomimetic regeneration. © 2000 Published by Elsevier Science B.V.

Keywords: Abalone shell; Biomimetics; Growth dynamics; AFM

1. Introduction

Biological hard tissues are excellent examples of hierarchically structured multifunctional composites [1–4]. These include bony (bones and antlers) and dental tissues (dentin and enamel), echinoderm skeletal units, sponge spicules, and a great variety of mollusc shell structures. Under the genetic control of organisms, these biocomposites are formed via energy efficient and environmentally friendly (but not yet fully understood) synthesis pathways. The lessons learned from the studies of structures and functions of biological hard tissues and their synthesis pathways have immense potential in both health and engineering applications [3–6]. On the one hand, they provided better insight into how bone and dental tissues might be regenerated [7–9]. On the other hand, biomimetic structural design criteria and novel processing techniques might be developed for functionally efficient and environmentally benign processing of new technological materials [3–6,10,11].

The interest in this paper is a biological hard tissue with a relatively simple microarchitecture constituting the shell of red abalone, *Haliotis rufescens* [12–14]. It is an example where nature has used readily available materials (e.g. Ca^{2+} and CO_3^{2-} ions) in seawater in order to generate a multifunctional composite material. The shell is a ceramic/biopolymer hybrid composite structure [14–16] with two microarchitecturally different sections. The ceramic component is $CaCO_3$ (in two mineralogical forms constituting the two sections of the shell) and the organic is composed of proteins (and, also, likely to contain lipids and polysaccharides). The outer region of the shell has the prismatic section (P) in which the calcitic (rhombohedral $CaCO_3$: $R3m$) crystallites are oriented perpendicular to the shell plane. The inner region has the nacreous section (N); here pseudohexagonal platelets (single crystals of microtiles) of aragonite (orthorhombic, $Pmmm$) are oriented parallel to the shell plane. The calcite crystallites are about a few micrometers in edge, and have an aspect ratio of about 5. The aragonite platelets have a thickness of 0.25–0.4 μm, and an edge length of 5 μm (aspect ratio of ≤ 0.1!). Some of these morphological features are shown in Fig. 1a, a scanning electron microscopy (secondary electron) image of a fractured surface across nacre (N)/prismatic (P) interface. While the prismatic layer

* Corresponding author. Tel.: +1-206-543-0724; fax: +1-206-543-6381.

E-mail address: sarikaya@u.washington.edu (M. Sarikaya).

0928-4931/00/$ - see front matter © 2000 Published by Elsevier Science B.V.
PII: S0928-4931(00)00202-2

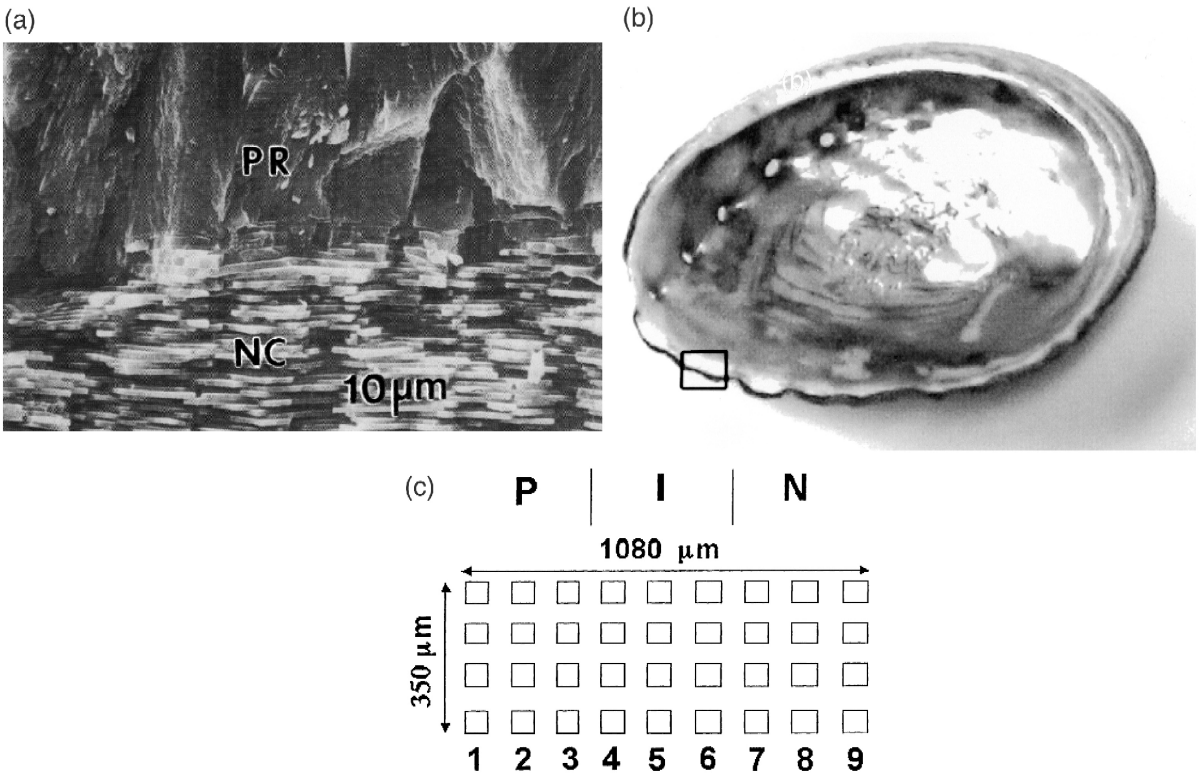

Fig. 1. (a) A SEM (secondary electron) image recorded from the interfacial region where the prismatic (PR) and the nacreous (NC) sections meet in a fully-grown section of an red abalone; (a fractured, cross-sectioned sample). (b) A photograph of the inside of a red abalone shell. The boxed area is the region of interest in this investigation. The lower dark region is the prismatic substrate and the lighter region above, within the circle, is the nacre, or "mother-of-pearl". (c) A diagram of the scanned surface. The numbers next to a row of four scans corresponds to the numbers given in Table 1.

provides the hardness, the nacreous layer, with alternating layers of aragonite platelets and organic film in between, provides the toughness to the shell. In both regions, the organic constitutes less than 5% by volume of the composites. This results in an "ideal" impact resistant material. Mechanical properties, crystallography and morphology of each of these sections of the hard tissue have been investigated [14–16].

The organic component, in particular, in the nacreous section of the red abalone shell, has been a topic of significant investigation [17–22]. First of all, the organic matrix (a thin film between aragonite platelets) is clearly an integral part of nacre, which is a hybrid composite materials system as it provides the soft component (for toughness) to the composite [14–16]. The role of the organic matrix on the formation of molluscan shells has been mostly related to its effect on mineralogy of the $CaCO_3$ [23–31]; however, how organic matrix directs the crystallographic and morphological growth of $CaCO_3$ units has been mostly conjectural (an issue still requiring careful consideration).

The multifunctionality of the mollusc shells originate from mineralogical, morphological, and crystallographical differences in the composite structures and how they might be correlated with each other. This, in particular, is more apparent in the inorganic component, i.e., $CaCO_3$, of nacre and prismatic composite sections in the abalone shell. As indicated, significant work has been performed on the crystallographic and morphological characteristics of the prismatic and nacreous regions [14–16,32]. However, these regions have mostly been studied separately, and there has been only limited correlation between the two sections.

The purpose of this investigation was simply to examine topographical features that may be specific to the nacre and the prismatic regions at the inner side of a growing edge of the red abalone shell. As we report in this paper, not only there are significant differences in the surface features in these two regions at the growth edge, but they can also be structurally and dynamically correlated with a simple mathematical model in relation to radial growth of the shell. That is, at a given particular location on the growth edge of the shell, topographical features follow a predictable pattern that can be related to either of the prismatic, nacreous, or the interface regions. Although growth in biological systems is a complex phenomenon involving many simultaneously occurring physiological processes, systematic examination of the surface microstructural development of a hard tissue, as demonstrated here, can produce data that could be used as a quantitative probe for dynamics of its formation. The growth model would be adapted (by, e.g., zoology) in shell morphogenesis, in biomimetic processing of organic/inorganic materi-

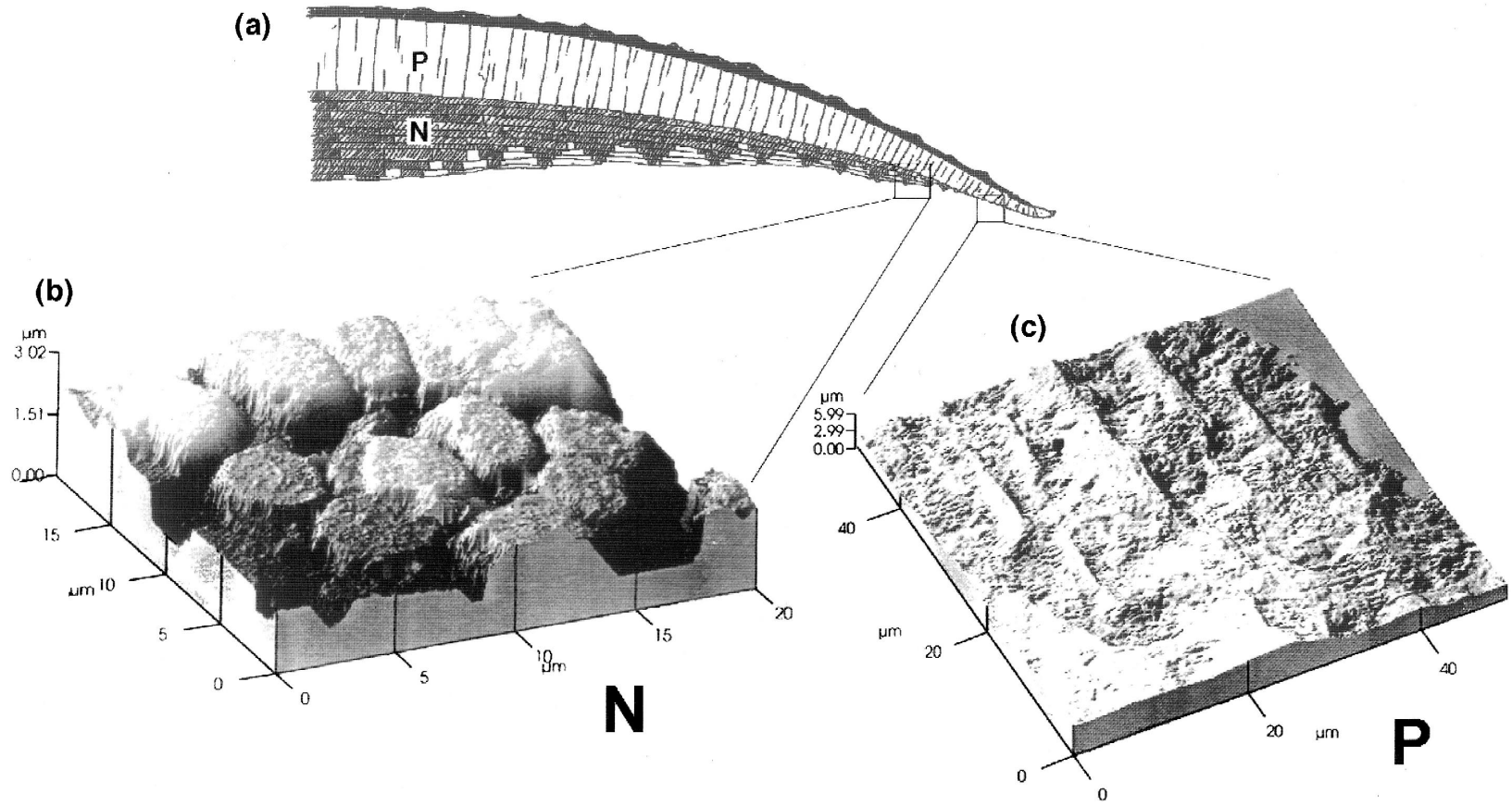

Fig. 2. (a) A sketch of the growing edge of abalone in cross-section (The sketch is based on our earlier investigation of the shell [16]). AFM images of the nacre and prismatic regions are also shown, in (b) and (c), respectively (see text for explanations).

als, and for hard tissue engineering (e.g., bone and dental tissues). The findings reinforce the ideas that when considering engineering of biomimetic materials, for example, one must not only evaluate structural and spatial relations but also the dynamics of a growth process. The relation between spatial and temporal scales must be addressed with regards to the processing of such materials. The results presented here give a quantitative (order of magnitude) estimate of such a time scale for the formation of a biological hard tissue.

2. Experimental approach

An atomic force microscope (AFM), Park Scientific, CP, was used to obtain surface topography using contact mode in air ($\sim$ 100 nN applied force). A red abalone shell of a moderate size (20 cm diameter) was used which was originally collected from Baja California. The growth region of the shell is identified as the peripheral line where nacre and prismatic sections overlap with a broad interface along the inside surface of the shell. This region of the shell will be referred to as the "growth-edge" throughout this paper because this is where nacre (located in the interior of the shell) meets the prismatic surface (located at a position of few millimeters of the periphery of the shell). The term "growth-edge" is used due to the fact that this region is the beginning of the edge, or lip, of the shell, which grows radially outward.[1] Fig. 1b photographed image of the inside of the shell showing an approximate region (Fig. 1c) of the shell investigated.

A schematic cross-section of the shell at the growing-edge is presented in Fig. 2a based on our previous investigation [16]. The shell in cross-section tapers off towards its periphery, exposing the latest-formed surfaces of both nacre (N) and prismatic (P) as they meet to form a transition zone across three regions, i.e., prismatic–interface–nacre (PIN). This zone across the interface is scanned by AFM showing characteristic microstructures on the growth surface of the shell which basically contains nacre microtiles (platelets) forming atop the prismatic section; these are described in detail below (Fig. 2b–c).

The shell sample for AFM investigation was mounted onto a steel disk and cleaned with deionized H_2O. A total of 36 images of 50×50 μm were scanned over a region of an approximately 350 (parallel to the growth edge) $\times$ 1080 μm (perpendicular to the growth edge) as schematically shown in Fig. 1c. The scans were taken in this manner to improve upon a statistical representation of the surface topography. The displacement from one scan to the next was measured by using the dimensions of the AFM cantilever. The silicon nitride (Si_3N_4 or Si) cantilever used is approximately 85 μm long and 60 μm wide at the base where it is attached to a silicon chip (ultralever, spring constant 2.8 N/m; Digital Instruments, Santa Barbara, CA). The AFM used in our laboratory has a light optical microscope ($1000\times$ magnification) which allows one to locate the cantilever's location with respect to the sample surface being profiled. Therefore, by choosing a point of reference, e.g., a particular feature on the surface, one can then translate the cantilever to another region with a quantitative measure of how much the cantilever has been displaced from one region to another.

Being able to differentiate between the nacre and prismatic regions is necessary as we are interested in profiling the region where nacre forms over prismatic calcite. It must also be noted that nacre of the shell discussed here is not a fully completed section, but in transition. That is, the surface is not completely flat (unlike, e.g., a cleaved nacre surface would have), but fairly so because of the presence of an organic layer at the topmost surface. Therefore, the surface of the shell at the growing edge, as moving from prismatic towards the completed nacre (i.e., from the outside of the shell to the inside), undergoes a rough-to-smooth transition. The model to be presented tries to predict at what point in time this section will become a flat (complete) nacre surface (i.e., the surface covered only with the organic layer). The prismatic region topographically consists of larger scale miscrostructural features, e.g., striations or ridges. These features on nacre and prismatic regions are presented in Fig. 2b and c, respectively. The AFM image recorded from the nacre surface away from the interface displays separately forming crystallites of pseudohexagonal aragonite microtiles that are fairly further along in their growth stage. An imaginary line profile taken across the newly grown nacreous surface would show fairly flat regions corresponding to the surface of the organic thin-film (which eventually becomes the organic matrix between the aragonite platelets) [17,18] and occasional "cusps" (nuclei) corresponding to the newly forming microtiles [16]. Fig. 2c is an AFM image of the prismatic surface where large-scale parallel striations, or continuous ridges, are apparent; these features contribute to the rough surface in this region.

3. Results and discussions

The topographical data was analyzed with respect to the rms (root-mean-square) roughness, z_{rms}. This surface parameter is given by the following equation where z is the "height" or deflection of the tip, $\bar{z}$ is the average height recorded, and n (integer) is the number of sampled regions. For this experiment, the sampled region was $256\times$

[1] When viewed from the top, the shell exhibits (logarithmically) spiral growth lines centered at the scarr, where the organism's foot is attached to the shell [24].

256. Note that the square of z_{rms} is just the topographical dispersion about $\bar{z}$ [34].

$$z_{rms} = \left[\frac{\sum_{i=1}^{n} (z_i - \bar{z})^2}{n-1} \right]^{1/2} \quad (1)$$

Table 1 displays the z_{rms} values obtained from the AFM results for the 36 scanned images. The nine values given correspond to the average value for a row of four scans parallel to the radial growth front starting with the region within the prismatic section. Fig. 3a is a plot of z_{rms} versus the spatial relation of the nine regions. The distance from the prismatic to the nacre region is approximately 1080 μm as stated previously. The distances between the centers of two neighboring images are roughly 100–110 μm.

From Fig. 3, we see that there is a trend for z_{rms} to decrease as we go from the prismatic region to the nacre region with a fairly flat plateau in between. It was thought that perhaps this trend may be due to the shell having a uniform non-zero slope derivative within a local prismatic region. When the long-range fluctuation ($\sim$ 50–100 μm) within the surface was removed with a first order plane fit removal (flattening), z_{rms} was shifted down from one region to the next (see Table 1, second column). The change in z_{rms} due to the first order plane removal may be a good measure of whether one is actually scanning within a region, which is more prismatic than nacreous due to the larger shift in the prismatic data compared to that of the nacre.

Since the inside "growth edge" surface of the red abalone shell, in fact, represents different stages of growth, the different regions, N, I, and P, may be related to each other via a model. This model, if found, could describe a spatial relation of these three regions with respect to a temporal scale. The model described herein explains this relation with regards to the change in the surface roughness of the growth edge of the red abalone. The prismatic region is rather rough in comparison to the newly grown nacre surface when one compares the values for z_{rms} given above for the three different regions. On a prismatic surface, there are ridges; but a freshly grown nacre has a smooth surface covered with an organic layer that spans between the tips of the pyramidal columns of stacked aragonite platelets (as seen in many SEM images in the literature) [16,24]. Since it is the rougher prismatic region that will eventually be covered with a smoother surface of nacre by aragonite formation, we can make the assumption that the nacre regions that were scanned were, at one point in time, a rough prismatic surface. Therefore, assuming that the AFM images within the nacre region were positioned on the prismatic substrate, we can then build the following time evolution model which will tell us how long it takes for the prismatic surface to be covered smoothly by the growth of nacre over it. The model would also provide a smoothing coefficient indicating a rate at which this process takes place. The purpose of the model is to measure the time scale of nacre growth on the prismatic region. This growth model could be helpful in understanding what time scale may be required in a biosystem with two hard tissues, whose microstructures may be coupled with an interface (e.g., compact versus porous bone [14] dentin versus enamel [9]), irrespective of the knowledge of the physiological conditions essential for the growth to occur.

From the abalone shell, histogram of the z_i measurements by AFM were generated for each of the 36 AFM scans. For the most part, these were found to be fairly Gaussian in nature (not shown) where z_{rms} is the HWHM (half-width half-maximum) of the Gaussian fit. It should be noted that the distribution shown below was normalized. A few histograms were found to have multiple maxima which are due to large (greater than 5 μm) periodic features within the topography such as the striations in prismatic region. One measure of whether or not

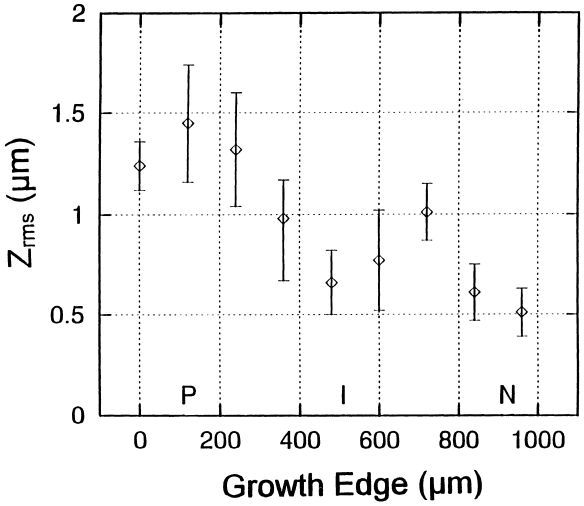

Fig. 3. z_{rms} versus the spatial relation of the regions whose rms roughness values are given in Table 1.

Table 1
Regions of analysis at the growth edge and corresponding z_{rms}

Region	z_{rms} (μm), raw	z_{rms} (μm), flattened	Δz_{rms} (μm)	Δz_{rms} (μm), average
1	1.24 ± 0.12	0.63 ± 0.35	0.61	
2	1.45 ± 0.29	0.66 ± 0.23	0.79	0.63
3	1.32 ± 0.28	0.83 ± 0.21	0.49	
4	0.98 ± 0.29	0.85 ± 0.22	0.13	
5	0.66 ± 0.16	0.38 ± 0.10	0.28	0.20
6	0.77 ± 0.25	0.58 ± 0.14	0.19	
7	1.01 ± 0.14	0.82 ± 0.16	0.19	
8	0.61 ± 0.14	0.50 ± 0.18	0.11	0.12
9	0.51 ± 0.12	0.44 ± 0.11	0.07	

the histogram is Gaussian is in the comparison of the median and mean z values. If these are equal, then a Gaussian fit may be appropriate. If these values are close, with a 4–5% difference, then one may be able to use a Gaussian fit as a first order approximation. For the values measured in this work, the average percentage difference was between 0.0% and 8.0%.

In order to make the model simpler, based on the information in Fig. 3 which displays three separate regions, the AFM scans were artificially summed into three different regions each having a projected area of approximately 350 μm parallel to the growth edge and by 360 μm perpendicular to the growth edge (Fig. 3). We take the prismatic region to be the first or initial region considering it to be a surface for nacre growth and to be the oldest of the three. The next region will be referred to as the interface (I) or transition region because it is here that we begin to see the formation of nacre microtiles (i.e., aragonite nuclei) on prismatic surface. The last region, where growth has taken place the latest on a time scale, is the nacre region. The data was collected in this manner in order to obtain a smooth statistical representation of the surface without much bias due to statistically unlikely irregularities. The HWHM for each region, based on the data in Fig. 3, is given in Table 2.

The variation of the height from the most probable, or mean, height will be referred to as the topographical variance [33,34]. This measure is not sensitive to the engaged height of the AFM tip because it is just a measure of height differences. The variable parameter for topographical variance will be z, with z' being the most probable height. Since we are assuming here that the surface will evolve to the one that is flat, with no topographical variance, then the height distribution eventually becomes a δ-function. The problem here is analogous to one of adsorption. Instead of having a δ-function source which spreads out over time, we have a system which is initially spread out and evolves to one described by a δ-function due to the topographical distribution becoming more concentrated over time. One solution to the diffusion equation in this analogy is in the form of a Gaussian as described below. In this case, we are interested in the solution where we have applied time-reversal symmetry due to our boundary conditions being reversed diffusion boundary conditions. Instead of having an initial time condition where the HWHM is 0, we now require this to be the condition for the final time, t'.

Table 2
Average values of z_{rms} through the interface

Region	z_{rms} (μm), HWHM
(P)rismatic	1.34 ± 0.23
(I)nterface	0.81 ± 0.23
(N)acre	0.71 ± 0.13

The Gaussian fit is not exact and in some cases it is skewed more than in others. The model presented here is meant to be a first order approximation. As stated previously, the z_{rms} is the HWHM of the Gaussian. The dynamic Gaussian is the following Green's function (G, i.e., a solution to the time-reversed diffusion equation), where z is topographical variance, t is time, and ε_s is smoothing coefficient [35]. The height distribution is normalized to about $x' = 0$.

$$G\left(x,t|_0^{t'}\right) = \frac{1}{z_{rms}\sqrt{2\pi}} \exp\left\{ -\frac{x^2}{2z_{rms}^2} \right\} \quad (2)$$

$$z_{rms} = \sqrt{2\varepsilon_s |t' - t|} \quad (3)$$

The choice in the form of the dispersion, z_{rms}, was made because it is believed that the growth of the nacre over the prismatic section may follow a diffusion law (random walk). For a one-dimensional random walk problem, the dispersion is just $\sigma = (Npq)^{1/2}$ where N is the number of steps and p and q are the probabilities of moving to the right or to the left. In our case here, the time interval $|t' - t|$ is representative of N, and the factor pq is representative of the smoothing coefficient ε_s. The value of p would be the probability of the surface of the nacre section smoothing out a given point in a local neighborhood, whereas q would be the probability of not changing, i.e., $1 - p$.

Now, we make the following assumptions in order to determine the smoothing coefficient ε_s as well as t'. The shell of red abalone grows radially by approximately 2.5 cm (1 in.) per year [1,2,13,32]. Let us assume this to be constant. We know that in reality the shell grows spirally [36,37]; nonetheless the edge of the shell moves with a net radial growth (i.e., the growth in the direction normal to the tangent at the edge). The radial growth velocity, v_g, is probably a function of many physiological variables, i.e., $v_g[\rho(Ca^{+2}), \rho(CO_3^2), T, P, \ldots]$, where $\rho(Ca^{2+})$ and $\rho(CO_2^{-2})$ are the solution concentrations of the inorganic components needed to generate the biominerals, and T and P are the local temperature and pressure of the animal's inner mantle surface [1,32]. This rate will also depend on the animal's diet with regards to the generation of the nutrients needed for the formation of the shell as well as synthesis, diffusion, and assembly of the macromolecules that make up the organic matrix of the shell. Therefore, our model is only an approximation giving us an order of magnitude for the values of the final time t' and the factor $2\varepsilon_s$.

One should recall that the prismatic surface is relatively the oldest of the three and that the nacre represents the newly formed surface. We can assume that the nacre region at one point in time was the same, or similar, to the interface region which itself was, at an earlier time, similar to the prismatic region. With this point in mind, we can now find the corresponding relative time of each region to be represented by the HWHMs listed above; we find the

Table 3
Three separate regions and the corresponding times at the growth-front

Region	t (days)
(P)rismatic	0.0
(I)nterface	5.2
(N)acre	10.4

following times where we set $t_p = 0$ days (time) and $p_p = 0$ μm (position) (where the subscript p stands for the center position of the region analyzed). This gives us $p_I = 360$ μm and $p_N = 720$ μm.

With the values for time t shown in Table 3, and the z_{rms} given in Table 2, we can now plot ε_s versus the final t' for each region. The section of the plot where the curves for the three regions cross determines a range of values for ε_s and t'. As one sees from Fig. 4, there is only a small section of the plot where this occurs. This region gives the unique solution of the three curves representative of the three regions P, I, and N. It must be made clear that for each of the growth-edge regions, there is a family of curves which lie within a range given by the uncertainly of the z_{rms} values. This is why one can see nine curves in Fig. 4. For each region (i.e., P, I, and N) there is actually an infinite number of curves between the representative upper and lower bound values and the one that represents just the absolute value of z_{rms}.

The area generated by the three sets of three curves (in Fig. 4) gives the range of unique solutions for ε_s and t'. The following equation is that of the curves in this spot.

$$\varepsilon_s(t) = \frac{z_{rms}^2}{2|t' - t|} \tag{4}$$

From the plots, the values for ε_s and t' were found to be; $\varepsilon_s = (0.042 \pm 0.005)$ μm^2/days and $t' = (16.5 \pm 2.5)$ days. The absolute values were chosen by picking a point near the center of the area of the region where the curves of the three regions cross (shaded area in Fig. 4). The uncertainty was found by taking the width of this area along the ε_s and t' axes. It must be noted that the matching of curves for three regions is much simpler than it would have been for nine regions. Therefore, it was beneficial to combine the original data into groups of 12 scans for each of the three defined regions for statistical purposes. This also helped to make the fit more tractable in finding the smoothing coefficient and final time for the generation of a flat (nacre) surface.

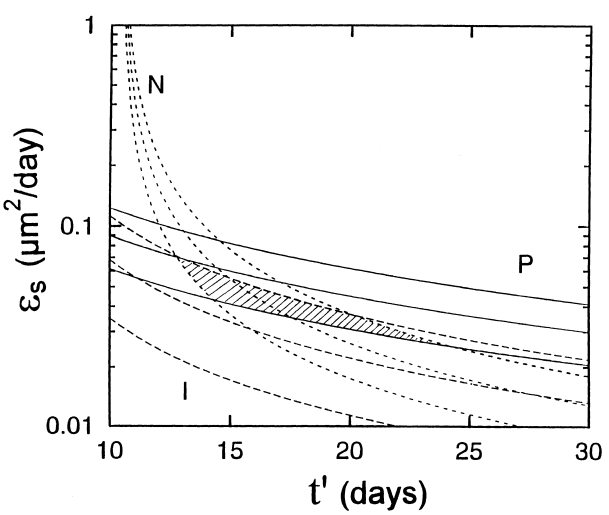

Fig. 4. Plot of the curves representative of the three regions P, N and I. There are three sets of three curves, one set for each region. The height and width of the shaded area give the unique range of values of ε_s and t'.

The ranges for z_{rms} of each region, predicted by the model, can now be back calculated using Eq. (3) for each region using the values found for ε_s and t'. The uncertainty of z_{rms} is given by the following where $\delta\varepsilon_s$ and $\delta t'$ are the uncertainties in the smoothing coefficient and final time, respectively. The corrected values are given in Table 4.

$$\delta z_{rms} = \left[\frac{|t' - t|}{2\varepsilon_s} \delta\varepsilon_s^2 - \frac{\varepsilon_s}{2|t' - t|} \delta t'^2 \right]^{1/2} \tag{5}$$

When comparing the measured z_{rms} to the calculated values shown below, we see that for the prismatic region, the calculated value tends to be at the lower end of the measured range. For the interface region, we have just the opposite. The measured and calculated values for the nacre region are practically the same.

With the corrected z_{rms} values, we can now plot the theoretical Gaussian curve representing the height distribution of the topographical scans for each region based on the experimental data applied to this model (see Fig. 5a). Each Gaussian represents the fit of 12 combined scans for each of the three regions P, I and N.

Most importantly, we are now in a position to place theoretical fit through the original raw data. The following equation is the analytical fit introduced by the mathematical model presented here. The fit consists of three curves; a best fit, lower bound, and upper bound. The zero point within the graph is not taken to be the same zero point for the calculation of the z_{rms} for the three regions P, I and N. One should recall that v_g is the radial velocity of the growth edge.

$$z_{rms} = \left[2\varepsilon_s |t' - x/v_g| \right]^{1/2} \tag{6}$$

Fig. 5b shows the analytical fit through the data. Notice that the curvature is negative. Therefore, this model pre-

Table 4
Predicted values of z_{rms} based on a one-dimensional diffusion model

Region	z_{rms} (μm), HWHM
(P)rismatic	1.2 ± 0.1
(I)nterface	1.0 ± 0.1
(N)acre	0.7 ± 0.2

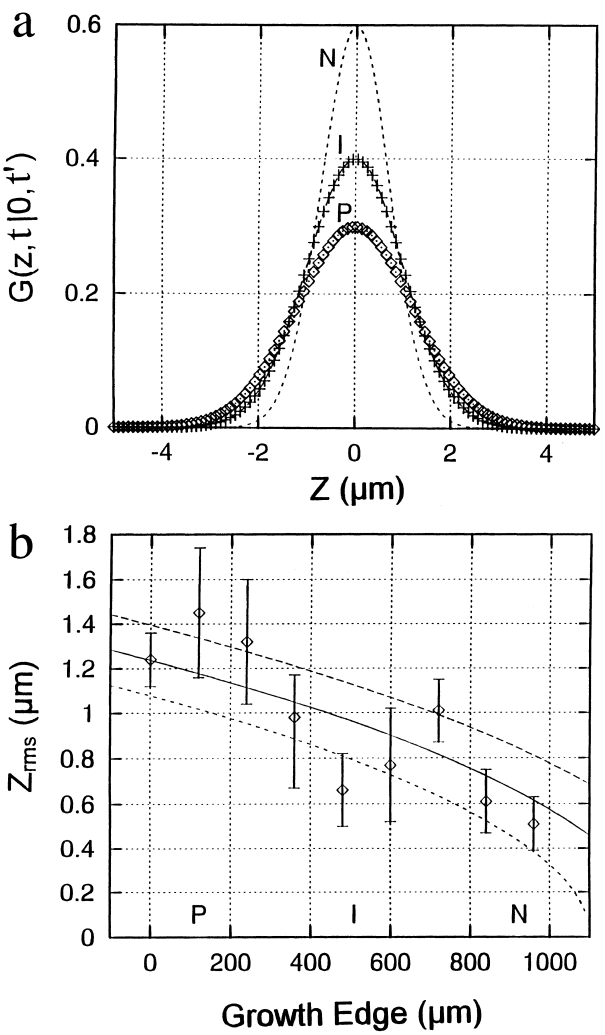

Fig. 5. (a) The Gaussian fit for the three regions, P, I, and N. Each fit represents the average of 12 AFM scans. (b) The analytical fit of the model through the measured data. The nonlinear curvature is due to the model being that of a diffusion law.

dicts that z_{rms} decreases faster as one goes from the prismatic region to the nacre region.

In the model presented here, a number of assumptions have been made that need to be recapitulated. It has been assumed that the radial growth of the shell is constant and linear. The height variation in a given region has been taken to follow one that is of a single Gaussian distribution. The three regions, P, I and N, have been taken to be such that the nacre region at one point had the same topography as the interface and that the interface at one point had the same topography as the prismatic region.

Nacre formation atop calcitic surface has already been observed on glass slip that was artificially inserted into the mantle of red abalone [38,39]. The model described here gives an insight into the understanding of generation of nacre region with the nucleation and growth of aragonite microtiles upon the biogenic prismatic surface composed of calcite grains constituting the shell of abalone. Our investigation does not give any information about a possible interaction between the organic matrix and either prismatic or nacreous regions of the shell. It does not take into account the fact that there is probably such an interaction. Nor it deals with any structural (i.e., crystallographical) or morphological (calcite striations in prismatic and aragonite on nacre) correlations between the inorganic phases of the two hard tissues. The rate of smoothing most likely also depends on the degree of structural correlation—via the organic matrix or inorganic phase interactions—between these two sections of the shell. The coefficient probably also depends strongly upon these interactions. Regardless, with this work, we have been able to extract temporal and spatial relation of the growth of the shell with a realistic assumption that the prismatic region possibly serves as a substrate for nacre formation, simply because on forms before the other, and that the two regions are intimately attached.

The mathematical growth model adapted here and its implications in correlating surface structural variations on the growth edge of abalone shell would be useful in biomimetics [3,5,6]. Abalone shell is a multifunctional material: outer (hard) prismatic and inner (tough) nacreous regions constitute sections of functionally gradient composite material [14–16]. For biomimetic regeneration of hard tissues or processing of synthetic materials, it is not only necessary to understand structural/mechanical relations of the desired biomimetic material, but also to have a measure of the time scale required to generate structural features with the length scales (nanometer, micrometer) of interest. On the one hand, more lessons learned from nature on the principles of biological synthesis of complex materials will eventually lead to their adaptation into practical engineering applications. On the other hand, the model may also be adapted to hard tissue engineering, such as bone or dental tissues. For example, like in abalone shell, human dental tissue consists of two separate regions, inner dentin and outer enamel, with fairly different microarchitectures and phase compositions [9,38]. The growth of enamel atop dentin may be likened to nacre growth over prismatic. Therefore, the model described here may also be useful in enamel biomimetics. It is reasonable to assume that, whether for practical engineering applications or for tissue engineering, nature's lessons will lead us materials scientists to rationally develop novel, environmentally benign, and multifunctional materials both for engineering [4] and health [40] applications in the near future.

4. Conclusions

Several points can be drawn from the results discussed in this work.

(i) Based on AFM roughness measurements, surface of prismatic (P) region of the growth edge of a red abalone

shell was found to be rougher (1.34 ± 0.23 μm) than the nacre (N) region (0.71 ± 0.13 μm). The roughness on prismatic surface corresponds to striations that have a spacing comparable to the that between centers of neighboring aragonite microtiles on nacre.

(ii) Based on a one-dimensional diffusion model for growth, the prismatic surface was theoretically found to be completely covered by the deposited nacre within $t' = (16.5 \pm 2.5)$ days with a smoothing coefficient of $\varepsilon_s = (0.042 \pm 0.005)$ μm^2/days. These parameters give z_{rms} values to be $P = 1.2 \pm 0.1$ μm and $N = 0.7 \pm 0.2$ μm, consistent with the experimental observations.

(iii) The theoretical results are based on the assumption that the deposition of nacre over the prismatic surface obeys a time-reversed diffusion law. The z_{rms} data agrees well with this assumption.

(iv) The model presented here may be useful in biomimetic development of multifunctional materials and in tissue engineering as it gives a temporal and spatial relation of the formation of one material (tissue) onto another.

Acknowledgements

This research was supported by an AASERT Program through ARO. Discussion with Dr. D.W. Frech was valuable.

References

[1] K. Simkiss, K.M. Wilbur, Biomineralization, Academic Press, New York, 1989.
[2] H.A. Lowenstam, S. Weiner, On Biomineralization, Oxford Univ. Press, New York, 1989.
[3] P. Calvert, S. Mann, J. Mater. Res. 23 (1988) 3801.
[4] I.A. Aksay, E. Baer, M. Sarikaya, D.A. Tirrell (Eds.), Hierarchically Structured Materials, Proc. of MRS, vol. 255, Materials Research Society, Pittsburgh, 1992.
[5] S. Mann (Ed.), Biomimetic Materials Chemistry, VCH Publishers, New York, 1996.
[6] M. Sarikaya, I.A. Aksay (Eds.), Biomimetics: Design and Processing of Materials, American Institute of Physics, New York, 1996.
[7] S. Wise, Eclogae Geol. Helv. 63 (3) (1970) 775.
[8] J. Glimcher, in: A. Veis (Ed.), The Chemistry and Biology of Mineralized Tissues: Wollf's Law Revisited, Elsevier, New York, 1981, pp. 617–673.
[9] J.P. Simmer, A.G. Fincham, Crit. Rev. Oral Biol. Med. 6 (2) (1995) 84.
[10] Materials Synthesis Using Biological Processes, in: P.C. Rieke, P.D. Calvert, M. Alper (Eds.), Proc. of MRS, vol. 174, Materials Research Society, Pittsburgh, PA, 1990.
[11] A.H. Heuer et al., Science 255 (5048) (1992) 1098.
[12] G. Bevelander, H. Nakahara, Calc. Tissue Res. 3 (1968) 84.
[13] H. Mutvei, Biominer. Res. Rep. 2 (1972) 48.
[14] J.D. Currey, J. Mater. Educ. 9 (1–2) (1987) 118.
[15] A.P. Jackson, J.F.V. Vincent, R.M. Tunner, Proc. R. Soc. London B234 (1988) 415.
[16] M. Sarikaya, I.A. Aksay, in: S. Case (Ed.), Results and Problems in Cell Differentiation in Biopolymers, Springer, Amsterdam, 1992, pp. 1–25, Chap. 1.
[17] M.A. Crenshaw, Biomineralization 6 (1972) 6.
[18] L. Addadi, S. Weiner, Proc. Natl. Acad. Sci. U. S. A., Biophysics 82 (1985) 4110.
[19] M.A. Cariolou, D.A. Morse, J. Comp. Physiol. 157B (1988) 717.
[20] S. Mann et al., Crystallization at organic–inorganic interfaces: biominerals and biomimetic synthesis, Science 261 (1993) 1286.
[21] A. Wierzbicki, C.S. Sikes, J.D. Madura, B. Drake, Calcif. Tissue Int. 54 (1994) 133.
[22] D.B. DeOliveira, R.A. Laursen, J. Am. Chem. Soc. 119 (1997) 10621.
[23] N. Watabe, J. Ultrastruct. Res. 12 (1965) 351.
[24] H. Nakahara, G. Bevelander, M. Kakei, VENUS (Jpn. J. Malac) 41 (1) (1982) 33.
[25] S. Weiner, W. Traub, Philos. Trans. R. Soc. London Biol. B304 (1984) 425.
[26] L. Addadi, S. Weiner, Mol. Cryst. Liq. Cryst. 13 (1990) 305.
[27] C. Furlong, R. Humbert, Proc. of MRS Symp., vol. 255, Materials Research Society, Pittsburgh, 1992, p. 435.
[28] L. Addadi, S. Weiner, Angew. Chem., Int. Ed. Engl. 31 (1992) 153–169.
[29] A.M. Belcher et al., Nature 381 (1996) 56.
[30] G. Filani, G.S. Albeck, S. Weiner, L. Addadi, Science 271 (1996) 67.
[31] D.A. Walters et al., Biophys. J. 72 (1997) 1425, March.
[32] K.M. Wilbur, in: K.M. Wilbur, C.M. Yonghe (Eds.), Physiology of Mollusca, vol. 1, Academic Press, New York, 1964, p. 243.
[33] J.M. Blakely (Ed.), Surface Physics of Materials, vol. II, Academic, New York, 1975, p. 476.
[34] T.R. Thomas (Ed.), Rough Surface, Longman, New York, 1982.
[35] P.M. Morse, H. Feshbach, Methods of Theoretical Physics, vol. 1, MacGraw-Hill, New York, 1953, p. 857.
[36] D.R. Fowler, H. Meinhardt, P. Prusinkiewicz, Modelling Seashells, Comput. Graphics 26 (2) (1992) 379–387.
[37] R. Giles et al., Biol. Bull. 188 (1995) 8.
[38] C. Zaremba et al., Proc. R. Soc. London 256 (1996) 17.
[39] C.E. Smith, Crit. Rev. Oral Biol. Med. 9 (2) (1998) 128.
[40] I. Martin, R. Quarto, B. Dozin, R. Cancedda, IEEE Eng. Med. Biol. Mag. 16 (2) (1997) 73.